Design and Manufacture of a Fuel Cell Powered Unmanned Air Vehicle

Unver Kaynak
TOBB University of Economics and Technology,
Department of Mechanical Engineering,
ukaynak@etu.edu.tr
Sogutozu, Ankara, 06560, Turkey

Rauf Akbaba, Alptekin Kibar
TESEM Inc.,
RAkbaba@tesem.com.tr, AKibar@tesem.com.tr
Ankara, Turkey

Coşku Kasnakoğlu, Nilay Sezer-Uzol, Emre Güleç, Semih Tekelioğlu, Mehmet Burak Solmaz
TOBB University of Economics and Technology,
Department of Mechanical Engineering,
kasnakoglu@etu.edu.tr, nsezeruzol@etu.edu.tr, st05150026@etu.edu.tr, st05150307@etu.edu.tr, st05150067@etu.edu.tr
Sogutozu, Ankara, 06560, Turkey

***Abstract*-This paper describes the methodology and building steps for a fuel cell unmanned aerial vehicle design and development carried out as a university-industry cooperation project. The concept design starts with the sizing of the aircraft based on parameters used for similar aircraft in the literature. The paper includes a spreadsheet based conceptual design methodology, power and propulsion analysis, stability and control analysis, development of an autopilot, CFD and FEM analysis, and the manufacturing processes using composites.**

I. Introduction

Fuel cell (FC) power plants are viable alternative to gasoline engine and battery driven electric motors because of high energy densities. Fuel cells can achieve nearly 1000 Wh/kg at system level whereas advanced batteries can reach energy densities around 150 Wh/kg [1]. This leads to development of fuel cell powered air vehicles designed for long endurance vehicles [2] or research motivated demonstration vehicles [3]. This paper concerns with the application of a proton exchange membrane fuel cell technology for a designed and manufactured short range Unmanned Air Vehicle (UAV). The project is carried out as a university-industry cooperation project between the TOBB University of Economics and Technology and TESEM Inc. in Ankara.

II. Concept design

Lessons learned study based on the past fuel cell aircraft configurations reveal a lot of guidelines about such vehicles. Based on such a study without going through a Response Surface Matrix or alike methodology, the following conclusions were drawn out for our concept:

Conventional geometry: A rectangular wing with a short fuselage and a single rear boom mounted empennage is selected. This concept is quite simple to manufacture and assemble compared to more sophisticated configurations.

Large Aspect Ratio Wing: FC power plants are still at their infancy based on the total Power/Weight (P/W) ratios regarding the total system weights. Therefore, large aspect ratios are necessary to reduce the induced drag for increasing the total performance.

Single Tractor Propellor: This system is a conventional single motor/propeller configuration that best fits the conventional geometry due to its simplicity. Its thrust characteristics are easy to predict and it also benefits from being lightweight.

Tricycle Landing Gear: It has the best directional stability property although it has some added weight and drag properties.

Based on these selections, Fig. 1 shows the conceptual drawing of the AKBABA UAV design.

II. Initial sizing

A spreadsheet program was developed for quickly calculating the overall flight parameters of the aircraft as shown in Table 1. The initial sizing of the aircraft was done based on Raymer [4] and Roskam [5,6] methods as shown in Table 2.

III. Aerodynamics

Aerodynamics studies regarding verification of some design choices and exploration of new subjects are done by using range of methods starting with the above given spreadsheet methodology, freely available web based methodology/ software, and finally using Computational Fluid Dynamics (CFD) methodology with different levels of detail. Wind tunnel and flight testing of the configuration design is the final stage of the process before going into a second and a third loops. Prior wind tunnel testing experience gathered at TOBB University of Economics and Technology (TOBB ETU)

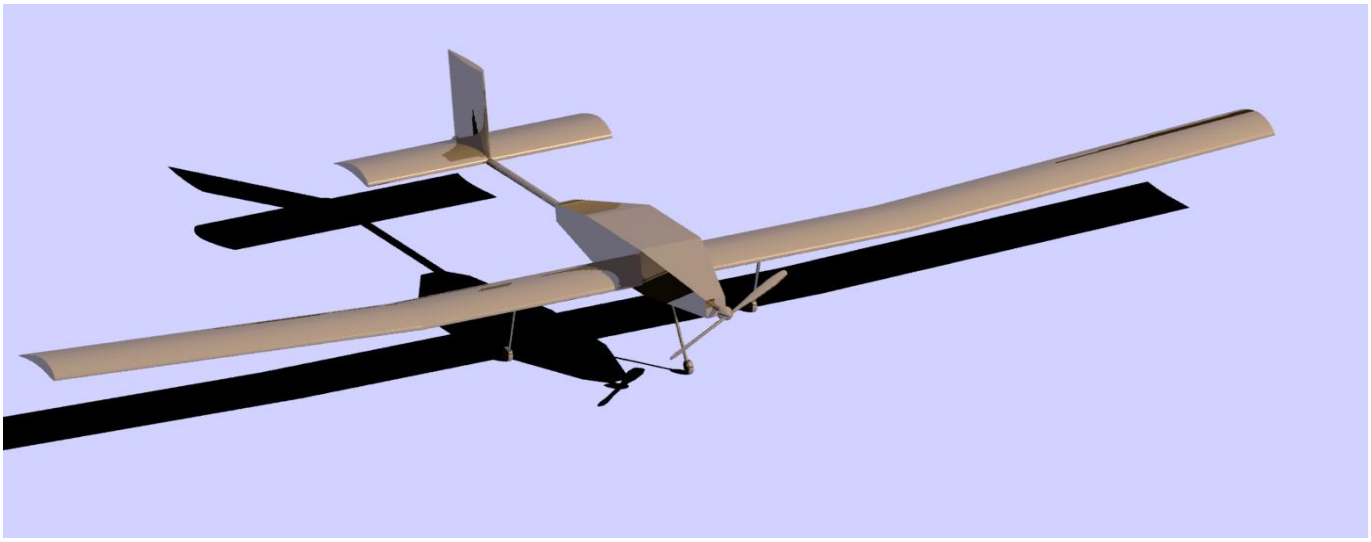

Fig. 1. AKBABA Concept Picture.

TABLE I Flight Dynamics Calculation Spreadsheet

	Flight Dynamics Equations								
	Fx =	**Tcos(teta)**	**- D cos(gamma)**		**- L sin(gamma)**				
	Fz = W -	**T sin(teta)**	**+ D sin(gamma)**		**- L cos(gamma)**				
WING	Gamma	Alpha	Theta	Weight (N)	Thrust (N)	Lift (N)	Drag (N)	Fx (N)	Fz (N)
	0	0	0	145	27	197.210	7.995	19.005	-52.210
	Rho (kg/m3)	V_cr (m/s)	K_vis	Cl_cruise	Cd0	Cd	Re		
	1.113	15	1.58E-05	0.9	0.015	0.036	324570		
	A.R.	e	T.R.	S_ref (m2)		b (m)	Cr (m)	Ct (m)	Cmac (m)
Eppler 420	15	0.8	0.9	1.75		5.123	0.360	0.324	0.342
FUSELAGE	A (T 6.3)	C (T 6.3)				L (m)	L_tail (m)		
	3.5	0.23				2.379	1.427		
HORIZ. TAIL	C_ht (T 6.4)	A.R.	T.R.			S_ht (m2)	b	Cr	Ct
NACA0009	0.5	4	1			0.210	0.916	0.229	0.229
VERT. TAIL	C_vt (T 6.4)	A.R.	T.R.			S_vt (m2)	b	Cr	Ct
	0.02	1.5	0.8			0.126	0.434	0.322	0.257

regarding the low Reynolds number airfoils and propeller technology sheds light into the present design. It is a well known fact that the tricky part of the airfoil selection is degradation of the airfoil performances in the low Reynolds number where viable predictions are difficult to make.

A. Airfoil Selection

Freely available web based softwares such as the JAVAFOIL [7] is used in the airfoil selection process. The marginal power output capacity of the current fuel cells stipulates us to use a high lift airfoil for the wing. Three candidate airfoils were chosen in the present project such as a very widely used model plane and UAV airfoil: Selig-Donovan SD7062, a general aviation airfoil: NASA LS(1)-0417, and a soaring plane airfoil: the Eppler420 [8]. The drag polar, coefficients of lift and moment versus angle of attack at a low Reynolds number of 300,000 are given in Fig. 2. Our past wind tunnel experience tells us that, in practice, the low Re number behavior may actually be worse then what is predicted here, but since the present approach is taken just as one of a trend analysis, this level of analysis is deemed sufficient at this stage. As seen, the E420 airfoil is a superior airfoil in terms of lift but with the attendant drag and moment penalties in comparison with the SD7062 and LS(1)-0417 airfoils. At this point, with regards to take-off and flexible loading requirements, the high lift character of the E420 overweighs the pitching moment and drag penalties, and therefore it is chosen as the design airfoil.

TABLE II Initial Sizing Results

INITIAL SIZING					
Component	**Input**	**Symbol**	**Reference**	**Entry**	**Unit**
Wing	airfoil lift curve slope	Cla	Javafoil	6.28	/rad
	mean aero chord	mac		0.340	m
	most aft cg location	Xcg		0.880	m
	cg_bar loc	X--cg		2.588	
	ac location	Xacw		0.850	m
	ac_bar loc	X--acw		2.500	
	ref area	Sw		1.750	m2
	exposed area	Sexp		1.700	m2
	aspect ratio	A		15.00	
	span	b		5.050	m
	1-M*2	beta		1.00	
	eta	Cla/2pi/beta		1.00	
	sweep	Λ_tmax		1.00	deg
Fuselage	% pos. of wing ac loc	Xacw / Lf		0.369	
	empirical pitch mom. fac.	Kf	Fig. 16.14	0.015	
	fus. width	Wf		0.250	m
	fus. length	Lf		2.302	m
	Diameter	d		0.250	m
H. Tail	airfoil lift curve slope	Clah		6.28	/rad
	ac location	Xach		2.200	m
	ac_bar loc	X--ach		6.471	
	Tail arm	Lt		1.350	m
	Upwash	d(eps)/dα	Fig. 16.12	0.200	
	Downwash	d(α_h)/dα		0.800	
	H.Tail eff.	eta_h	Eq. 16.6	0.900	
	ref area	Sh		0.210	m2
	exposed area	Sexp		0.210	m2
	aspect ratio	A		4.000	
	span	b		0.916	m
	1-M*2	beta		1.000	
	eta	Cla/2pi/beta		1.000	
	sweep	Λ_tmax		0.000	deg

B. CFD Simulation

Next level of prediction is carried out through viscous CFD methodology based on Reynolds Averaged Navier-Stokes equations. First, the validation of the low order airfoil results is done with the viscous and turbulent flow simulations using the ANYSYS CFX software [9]. Fig. 3 shows the mesh structure around the E420 airfoil using a total of 125,528 node points. Range of different turbulence models such as the algebraic model, two-equation standard *k-ε* model, *k-ε* RNG model, *k-ω* SST model and SSG Reynolds stress model are used. Fig. 4 shows the pressure contours and velocity vectors around the E420 airfoil at the Re number of 350,000 using the *k-ω* SST model. Note the high suction field on the airfoil upper surface that translates into a high lift airfoil. Table III shows a comparison of the lift and drag coefficients for the different turbulence models used at an angle of attack of zero degrees and a Reynolds number of 350,000. As shown, there is a good agreement between the *k-ω* SST and SGS Reynolds stress models in terms of the lift coefficient, and there is a good agreement between Javafoil and *k-ε* models in terms of the drag coefficient. Also, the 3-D CFD simulation was done using a coarse mesh of nearly 2,800,000 elements for an angle of attack of 0° and Re of 350,000 in order to have an opinion about the three-dimensional flow field around the UAV. Fig. 5 shows the unstructured tetrahedral mesh around the aircraft. Fig. 6 shows the surface pressure field and streamlines around the airplane where the red color indicates pressure regions and green and blue colors indicate suction regions.

TABLE III Comparison of different turbulence models at Re = 350,000.

	Cl	**Cd**
Javafoil	1.40	0.030
Algebraic	1.14	0.065
Standard k-ε	1.07	0.030
RNG k-ε	1.08	0.029
k-w SST	1.23	0.019
SSG Reynolds Stress	1.33	0.008

IV. Propulsion

Principles of electric design of an UAV require a combination of some analytical, numerical and experimental tools including a sensible data base especially for the propellers at low Reynolds numbers and a correct fuel cell/battery electrical power-electric motor-propeller combination. Especially, such a combination gets more tricky with the increase in altitude. In this project, our design process starts with the selection of a commercially available fuel cell system that imposes the maximum take-off weight and maximum take of thrust requirements. As current commercially available fuel cells may not be sufficient for all take-off and climb conditions, additional battery power should be accounted for. After the selection of the fuel cell system, pre-design of the electrical system is carried out by using another in-house spreadsheet methodology given in Table IV. The spreadsheet methodology is calibrated against legacy propeller data (Fig. 7) available in the literature [10]. The preliminary sizing of the propulsion system is finally checked against the web based freely available software: JAVAPROP [11]. Thrust and torque output of the propeller calculated by using the JAVAPROP software is shown in Fig. 8.

V. Stability and Control

Analysis of the longitudinal static stability and neutral point calculation is done via a spreadsheet program as shown in Table V. The aircraft is presently has a stick fixed static margin of 8%.

VI. Autopilot Design and Development

The freely available MATLAB/SIMULINK tools FDC [12] and Airlib [13] are used to develop an autopilot and simulate the dynamics of the controlled motion based on a nonlinear aircraft model.

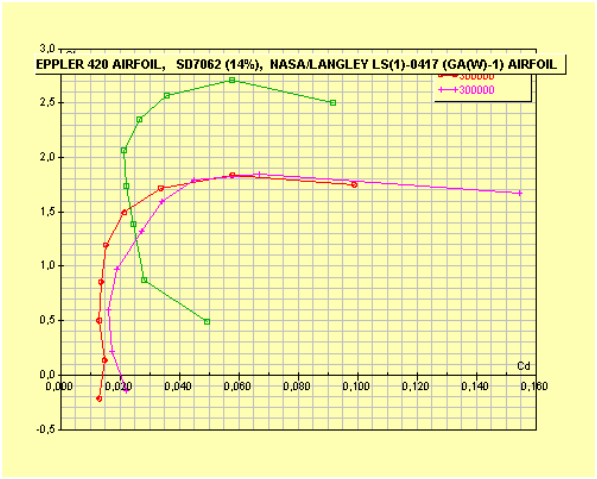

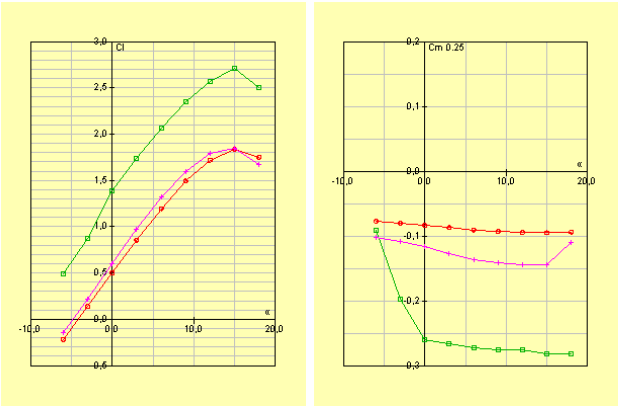

Fig. 2. Comparison of the drag polars, lift and moment coefficients of the E420, SD7062 and LS(1)-0417 airfoils at Re = 300,000.

Fig. 3. Mesh structure around Eppler 420 airfoil for CFD analysis

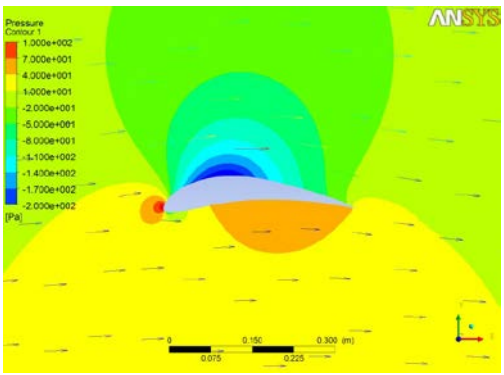

Fig. 4. Pressure contours and velocity vectors around the Eppler 420 airfoil at at Re = 350,000 using the k-ω SST model.

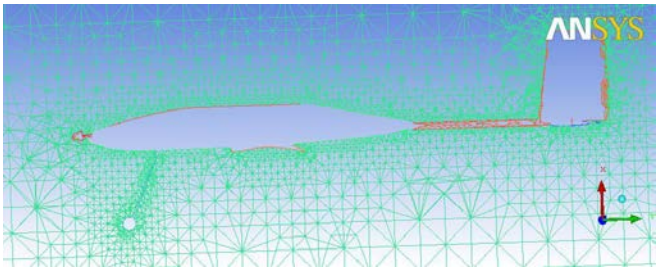

Fig. 5. Unstructured mesh around the UAV.

Fig. 6. Pressure contours on the surface of UAV at Re = 350,000.

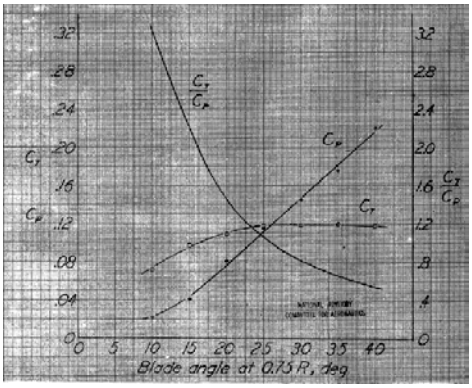

Fig. 7. Legacy data for a wooden two-blade propellers [10].

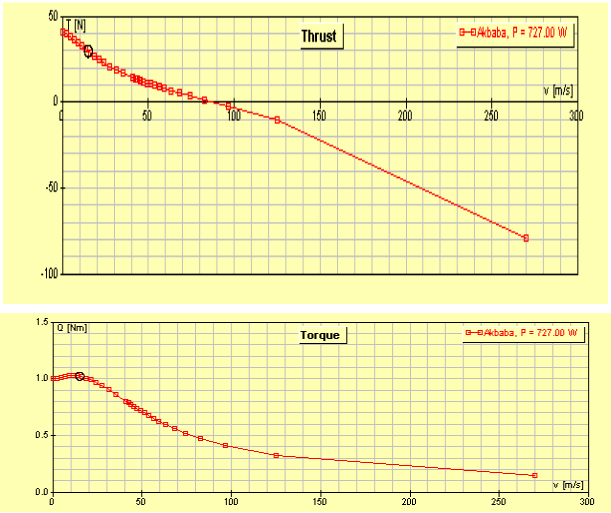

Fig. 8. Thrust and torque output of a propeller by using the JAVAPROP.

TABLE IV Spreadsheet program for calculating the electrical power and static/cruise flight thrust requirements.

POWER AND THRUST CALCULATIONS		
Aicraft		
W	150	N
b	5	m
C	0.34	m
Ro	1	kg/m3
v	15	m/s
S	1.7	m2
AR	14.7	
Cl	0.78	
Cd0	0.027	
Cm	-0.2	
E	0.8	
Cd total	0.044	
Drag	8.35	N
Lift	150.00	N
Moment	-13.01	Nm
P cruise, (prop) (req)	125	W
Efficiency (elec, mech)	0.79	
Efficiency (prop)	0.48	
Req cruise power	**329**	**W**
Motor		
I operating	50	A
I idle	2.5	A
R	0.03	Ohm
V	18.5	V
Power (shaft)	808	W
Power (motor)	925	W
Efficiency (elec)	0.87	
Efficiency (mech)	0.90	
Total Efficiency	0.79	
Available Power at shaft	**727**	**W**
Static Conditions		
Kv	400	rpm/V
rpm	6800	
rps	113	
Gear ratio	1	
n prop	113	rps
Diameter prop	0.406	m
J advance ratio	0.326	
Cp	0.045	
Ct/Cp	2.713	
T static	43	N
Loss factor	0.9	
Output Static Thrust	**39**	**N**
Flight Conditions		
Flight Power (absorbed)	**517**	**W**
Flight Thrust (available)	**23**	**N**
Prop Efficiency	0.48	

The autopilot designed keeps the velocity, altitude and the heading of the aircraft at desired reference values and also achieves coordination during turns by minimizing the lateral force acting on the aircraft. A schematic block diagram of the autopilot is shown in Fig. 9.

TABLE V Spreadsheet program for the neutral point calculation

STABILITY (STICK FIXED AND FREE)		
Formulas	**Reference [5,6]**	**Results**
Wing terms		
1+tan(Λ_tmax)*2/beta*2	Denom. Eq. 12.6	1.00
√4+A2beta2/eta2(1+tan())	Denom. Eq. 12.6	15.14
Wing CLa	Eq. 12.6	6.30
Fuselage terms		
F=1.07(1+d/b)*2	Eq. 12.9	1.18
Kf*Wf**2*Lf/mac*Sw	Eq. 16.22	0.004
Cma_fus	Eq. 16.22	0.208
Tail terms		
1+tan(Λ_tmax)*2/beta*2		1.00
√4+A2beta2/eta2(1+tan())		4.47
H.Tail CLah	Eq. 12.6	3.88
Neutral Point Calculation		
Cm-Tail effect	Eq. 16.9	0.34
Numerator (Stick-fixed)	Eq. 16.9	17.71
Denomerator (Stick-fixed)	Eq. 16.9	6.63
Numerator (Stick-free)	Eq. 16.9*tail fac 0.8	17.27
Denomerator (Stick-free)	Eq. 16.9*tail fac 0.8	6.57
Stick-fixed Stability		
Xnp_bar	Eq. 16.9	2.670
Xnp		0.908
Static Margin	Xnp_bar - Xcg_bar	0.081
Cm_alf	Eq. 16.10	-0.512
Stick-free Stability		
Xnp_bar	Eq. 16.9*tail fac 0.8	2.631
Xnp		0.894
Static Margin	Xnp_bar - Xcg_bar	0.042
Cm_alf	Eq. 16.10	-0.267

MATLAB/SIMULINK simulations performed with this autopilot in the loop are shown in Figs. 10 and 11. The scenario considered for these simulations is as follows: The designed UAV aircraft (as seen in Fig. 12) is flying at a speed of 20 m/s and altitude 1000 m. Between t=100 to t=200 seconds the autopilot is commanded to increase the altitude to 1100 m. The aircraft is instructed to fly at this altitude between t=200 and t=500 seconds and it is commanded to descend back to 1000 m between t=700 and t=800 seconds. After this, the autopilot is ordered to navigate the aircraft within a distance of 20,000 m of a runway located at coordinates (0 m, 30,000 m) oriented 150^{o} with the horizontal axis. Next, the autopilot is commanded to initiate the landing procedures, which involves descending 1000 m to land on the runway while at the same time reducing the velocity to the landing speed, which is about 10 m/s. Observing Figures 10 and 11, it can be seen that the autopilot achieves these commands described satisfactorily. Work is now in progress by the TOBB ETU Aviation Club ETUHAVK to build and test this autopilot experimentally.

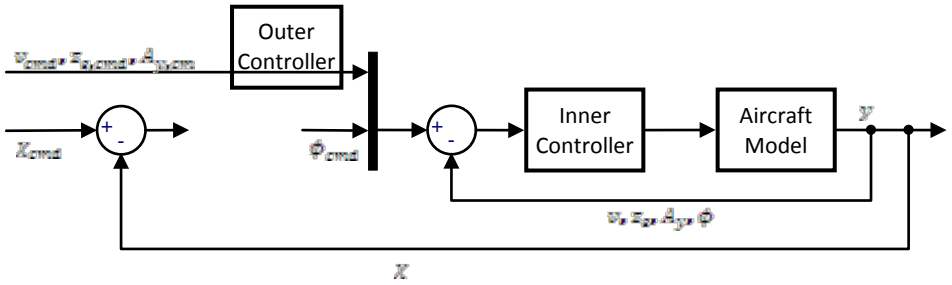

Fig 9. Closed loop system structure for autopilot design.

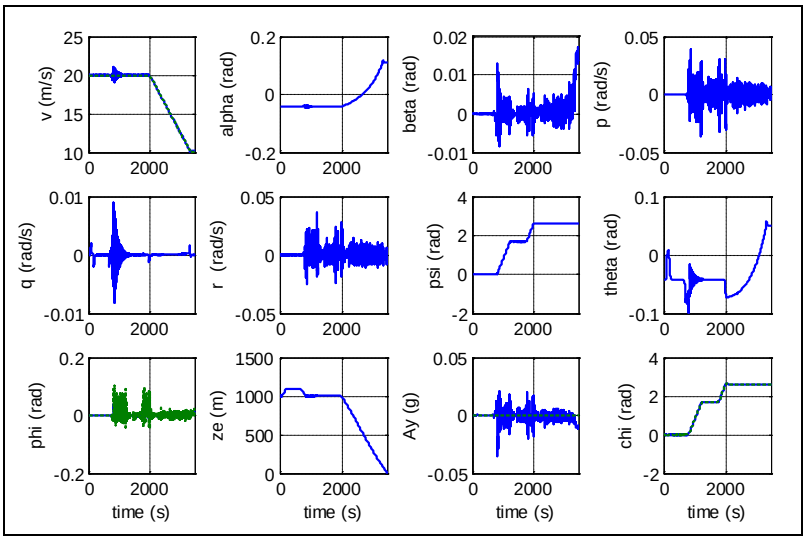

Fig. 10. Aircraft states resulting from SIMULINK simulations of the nonlinear aircraft model in closed-loop.

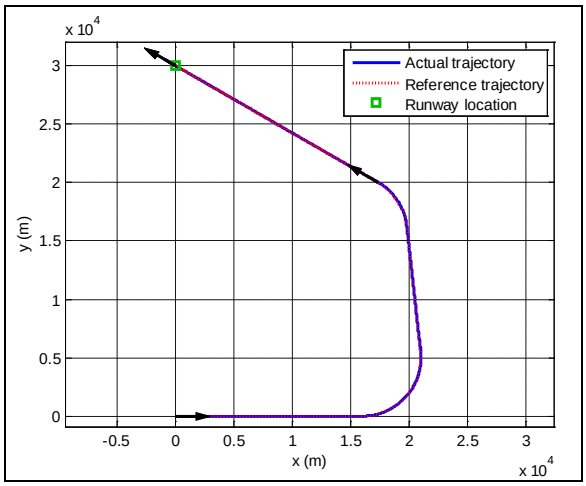

Fig. 11. Aircraft trajectory resulting from SIMULINK simulations of the nonlinear aircraft model in closed-loop.

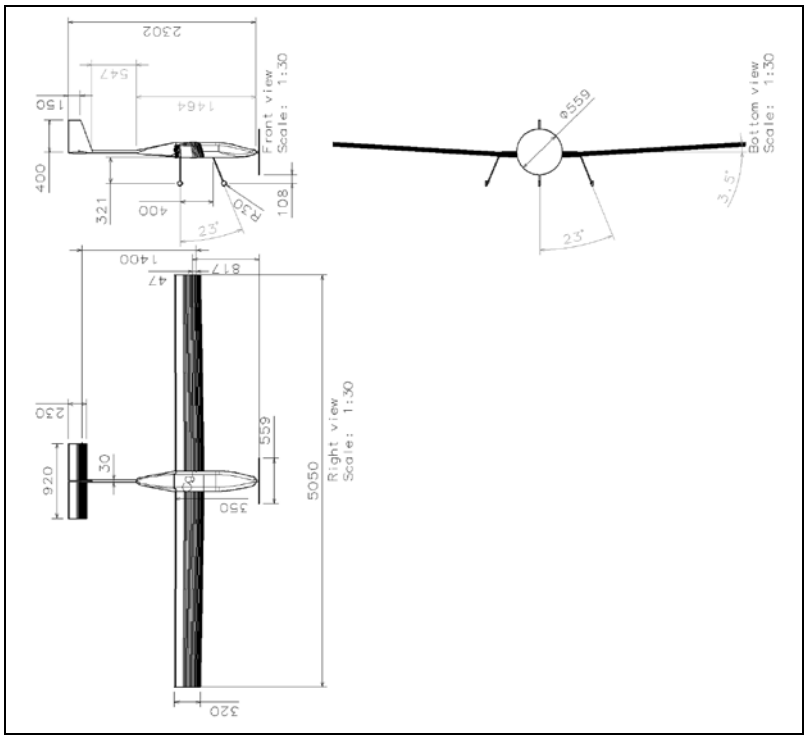

Fig. 12. Three views of AKBABA UAV.

VII. MANUFACTURING PHASE

Manufacturing phase was started with the development of the CAD model and drawings followed by the selection of the material and manufacturing processes. Since the aircraft must be light, in order to increase the efficiency of flight and decrease the costs (which are defined in design goals), the materials and mechanical systems must be considered well. As it is obvious, composite materials have good behaviors and most preferred ones for civil aircrafts. However they are rather expensive and a good way of making an aircraft with an electrical motor depends on its low weight. In the interest of building a composite body and wings, the three views of the aircraft are drawn using CATIA V5 [14] which can be seen in Fig. 12. After this step, core material is chosen as polystyrene. Polystyrene is a type of foam and the most useful one for this kind of airplane. Polyurethane and polyvinyl chloride were other options for core material but polyurethane is dangerous when it catches fire and polyvinyl chloride is not useful for big parts. Fabric cloth choosing is other important part of the manufacturing. In most composite aircraft, there are four different materials; fiber glass, Kevlar, carbon fiber and boron. Fiber glass is chosen in this project. Since this is an academic study, the prices are very important. Fiber glasses' mechanic properties are proper to manufacture a UAV because it is light, it has a high electromagnetic conductivity, it has endurance to atmospheric conditions, and also its price is optimum considered to its properties. There are three common types for fiber glasses E-glass, C-glass and S-glass. C-glass has a high corrosion, however, it has a low mechanical properties. The E-glasses have low elasticity and high fatigue strength. They are cheaper but they have also less strength than the S-glasses. S-glass types are 25-30% stronger than E-glass while they still carry all of the properties of E-glass and statically S-glasses can be loaded more than E-glasses. Resin making has a key role in composite aircraft building. Resin carries whole loads and also may give extra strength against bullets in military usage. In this project, three of resin types are considered; vinley ester resin, epoxy resin and polyester resin. Polyester resin is not proper for aircrafts. Although vinley ester resin has superiority in using time and prices, it may be explosive while mixing with cobalt nepthenate and methyl ethyl ketone peroxide. Since epoxy resin is widely used in aerospace industry and has good behaviors in both mixing phase and using phase, it has been chosen as the resin type to be used. Epoxy resins are usually used in coating and fiber glass composites. Heat processed epoxy resins have high strength and high chemical resistance and heat resistance.

There are a lot of options to make a composite aircraft since there are lots of brands and products. To make the selection simpler, international shops removed from the list because of their disadvantageous in shipping. Only the shops of composite material sellers are searched to get data. Hexion L285 for epoxy resin is more proper for aircrafts and its best match for aircraft building is Hexion H285-H287 epoxy hardener. Since there is no great difference in efficiency, H285 was chosen for its better price. The only proper option for epoxy paste is the Araldite. However there are many options for fiber glass fabric but only one of them is S-glass. Hence, Atlas S2 (190 gr/m2) as the Fiber Glass Fabrics, Hexion-L285 as the Lamination Epoxy Resin, and Hexion-H285 as the Lamination Epoxy Hardener are chosen.

The manufacturing technique will be handy lay up method to complete the assembly. By these selections, composite type is become clear. Using fiber glass with epoxy resin is defined as Glass Reinforced Polyester (GRE). Some mechanical properties of GREs are given in Table VI which shows that using fiber glass with epoxy resin is going to assist the structure very well while not having so much weight. This is also going to decrease the loads. While lower price is a crucial part of manufacturing, easy manufacturing is also crucial. The easier manufacturing means lower prices. So some design parameters have been changed by considering this. Taper ratio of the vertical tail changed to 1 to build it up easier. Because, if the taper ratio is different than 1, the cross section area of the tail will vary along its length and this makes its manufacturing harder. Also, the fuselage has changed to a simple and inorganic form. Before the conceptual simplification, the fuselage had various curves on it to give a more aerodynamic form which was more complex than its simplified form and was very difficult to be built by using hot wire cutter or some kind of different cutters. Fig. 13 shows these different forms. This modification decreases its aerodynamic performance, but this decrease is not so crucial at this stage of the project.

Table VI. Some properties of GREs which consist 50-80% of glass of continuous fibers [15].

	GRE
ρ [g/cm3]	1.6 - 2.0
E [GPa]	30 – 55
σ [MPa]	600 – 1165
σ_press [MPa]	150 – 825

A. FEM Analysis

Considering that the aspect ratio of the AKBABA UAV is 15, it can be foreseen that the greatest stress appears at the intersection between the wing and the fuselage because of the maximum moment that is produced by the lift force. Therefore, the structural Finite Element Method (FEM) analysis is concentrated on that region. According to the AKBABA Design Book, the foreseen weight is 145 N and this weight will be loaded on wings. A load factor of 3 was used as a safety factor in FEM analysis, so the new force is assumed 450N and this is divided by 2 to find one wing load. This force is distributed on the wing in parabolic form. For the FEM analysis, CATIA V5 software is used, because it is easy to transfer from the conceptual part design, which is also done using CATIA, to the analysis design or vice versa.

First, the surface meshing is done with a mesh clustering where the maximum stress expected to occur and the number of nodes is 33,805. The distributed force is applied on the surface area of the wing and the wing is fixed at the intersection between the wing and fuselage. A new material is selected which has required properties of S-glass and applied to the solution part. Also, inner foam is not applied because of its lower yields

strength compared to fiberglass. Its task is only to support the coating. So, the crucial point is the stress on fiberglass coating. Also, drag force of 4 N is applied as a distributed force. As a result of pitching moment, there must be a moment loading on wing and it is calculated for the cruise velocity of 20 m/s of UAV. According to this calculation, moment of 14 Nm is applied on the wing. The loading is shown in Fig. 14. It is observed from the FEM results that the maximum stress occurs at the upper surface of intersection region and its value is 62.32 MPa as shown in Fig. 15.

In Table VI, σ_{press} is stated between 150-825 MPa and to calculate the safety factor, 150 MPa is accepted for allowable stress. So the safety factor is 2.4 and this value is satisfying for the UAV design. From the FEM analysis, displacements of nodes are known and maximum displacement is seen to be 26.2 mm at the tip of wing. By dividing this to the length of the wing, displacement angle is found as 0.6° and this is acceptable for wing. In addition to this, because of the displacement, a twist angle occurs on the wing. At the tip of the wing, the twist angle caused by the loads is 0.046° and this is also acceptable. Further detailed FEM analysis will be done for the wing by using other FEM softwares. Also some analysis will be done for the landing gear. During take-off and landing, the gravity force of the UAV will be loaded on the landing gear. The landing gear must resist to this kind of load. Also, the parts where the landing gear connects to the UAV must resist to the take-off and landing loads.

VIII. Conclusion

A short range fuel cell powered UAV design conducted as a university-industry cooperation project is introduced. The AKBABA Design Book and the design steps are described and some results of the detailed CFD and FEM analyses are discussed. The development and manufacturing phase is presently under way.

References

[1] Anderman, M., "Brief Assessment of Improvements in EV Battery Technology Since the BTAP June 2000 Report," California Air Resources Report, 2003.

[2] AeroVironment Pres. Release, "Aeronvironment Flies World's First Liquid Hydrogen Powered UAV," June 28, 2005.

[3] Moffitt, B.A., Bradley, T.H., Parekh, D.E., and Mavris, D., "Design and Performance Validation of a Fuel Cell Unmanned Aerial Vehicle", AIAA Paper 2006-823, 44th AIAA Aerospace Sciences Meeting and Exhibit, Jan 9-12, Reno, Nevada, 2006.

[4] Raymer, D.P., *Aircraft Design: A Conceptual Approach*, 4th ed. Reston, VA, AIAA, 2006.

[5] Roskam, J., *Airplane Flight Dynamics and Automatic Flight Controls: Part 1*, Lawrence, KS, Design Analysis Research Corporation, 2007.

[6] Roskam, J., *Airplane Design Part VI: Preliminary Calculation of Aerodynamic Thrust and Power Characteristics 2*, Lawrence, KS, Design Analysis Research Corporation, 2000.

[7] JAVAFOIL, http://www.mh-aerotools.de/airfoils/javafoil..htm, April 2010.

[8] Selig, M., Coordinate Database, http://www.ae.illinois.edu/mselig/ads/coord_database.html#E, April 2010.

[9] ANYSYS CFX, http://www.ansys.com/products/fluid-dynamics/cfx/, April 2010.

[10] Gilman, J., Jr., "Static Thrust and Torque Characteristics of Single and Dual Rotating Tractor Propellers," NACA, Memorandum Report, Langley Field, VA, 1944.

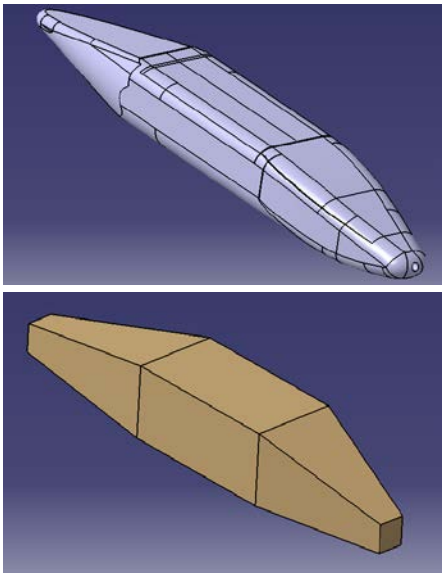

Figure 13. Fuselage forms before (top) and after (bottom) modification.

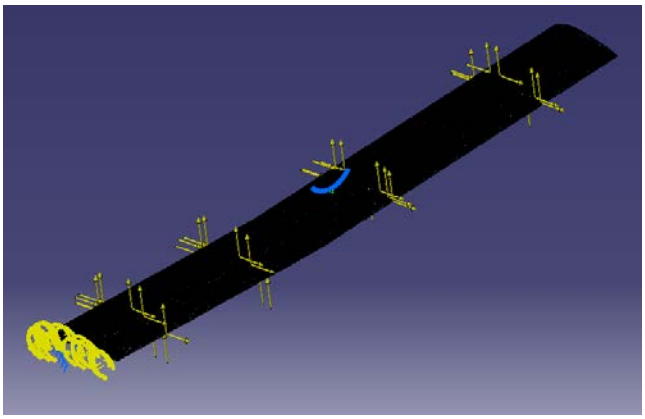

Fig. 14. Loads on the wing.

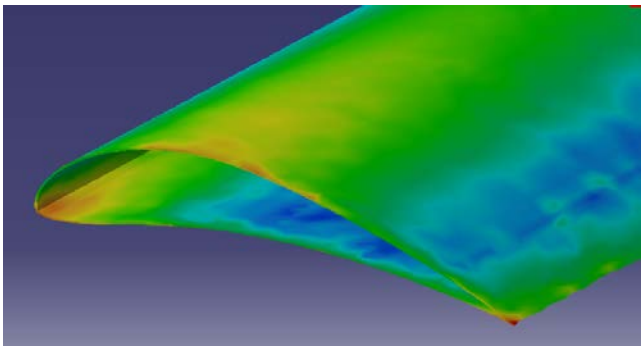

Figure. 15. Stress distribution at the intersection region.

[11] JAVAPROP, http://www.mh-aerotools.de/airfoils/javaprop.htm, Download.

[12] Rau, M., "FDC 1.2 – A Simulink Toolbox for Flight Dynamics and Control Analysis", 2nd Edition, May 10, 2001, http://www.dutchroll.com.

[13] Campa, G., "Airlib", http://www.mathworks.com/matlabcentral/fileexchange/3019-airlib, February 13, 2003.

[14] CATIA, Software Package, Dassault Systemes, Vélizy-Villacoublay, France, 2008.

[15] Übeyli, M., *Composite Materials Course Notebook*, Fall Semester, Dept. of Mechanical Engineering, TOBB ETU, 2009.